Vol. 36, No. 4 (2014) 451-464

Tribology in Industry

www.tribology.fink.rs

RESEARCH

Micro-lubrication of Directionally Oriented Contact Surfaces

O. Maršálek[a], P. Novotný[a], P. Raffai[a]

[a]*Institute of Automotive Engineering, Faculty of Mechanical Engineering, Brno University of Technology, Czech Republic.*

Keywords:

Asperity radius
Contact pressure
Flow factor
Fractal dimension
Rough surface

Corresponding author:

Ondřej MARŠÁLEK
Institute of Automotive Engineering,
Faculty of Mechanical Engineering,
Brno University of Technology,
Czech Republic
E-mail: marsalek@fme.vutbr.cz

A B S T R A C T

A description of the set of software tools for detailed computational modelling of thin lubrication layers behaviour is presented in this paper. Individual chapters outline reasons for realization of its each part, explain the functionality of each software tool and the given mathematical definition or digital implementation of all important equations or formulae. The following are examples of partial results of the analysis carried out and the resulting flow factors databases for some kinds of rough surfaces, together with an example of the analysis result of the connecting rod sliding bearing of supercharged internal combustion engine.

1. INTRODUCTION

All technological processes leading to the final surface design of mechanical components creates on its surface characteristic pattern. These surface patterns subsequently play, particularly in the case of surface contact pairs, a significant role in terms of their function and lubrication. However, inclusion of the actual surface patterns of machine parts, as one of the input parameters of the computational simulation of friction losses, does not even matter in the contemporary modern era. The current state follows logically from history – these detailed contact analyses could not be used effectively in the past due to their large computational complexity.

However, as time progresses also the computer technology has improved noticeably. Therefore, computational models also need to adapt to the contemporary hardware, to maximally exploit its potential and enable the emergence of more comprehensive, as well as, more sophisticated software tools. This statement is supported by the fact that development, especially the employment of experimental tools, is very expensive and time consuming in comparison with the application of computational models. These models, after completion, provide results quickly and inexpensively.

The perfection and credibility of the design of individual components nowadays plays an important role in the development of any

product already in the process of the virtual prototype. Therefore, the continuous improvement of computational models and their adaptation to the possibilities of contemporary computer technology, still more significantly, finds its application.

The description of advanced computational tools for investigation of frictional losses of mechanical tools will be described below, as it is a logical progression when its function is taken into consideration.

2. ROUGH SURFACES

To obtain the relevant data characterising the rough surface of real machinery parts, there are basically two following options: data obtained from the measurement (profilometer, scanner) or generated surface roughness profile.

2.1 Surface roughness measurement

Both alternatives for obtaining the surface roughness characteristics, mentioned above, have naturally their positives and negatives. Main disadvantages of the surface roughness measurement are e.g. the need to purchase expensive measuring equipment, large time-consumption, or the dependence on the realisation of a real sample.

On the other hand, the advantage of this option is that (if the sufficient measurement accuracy is provided and also the meaningfulness of subsequent filtration is guaranteed) we have real data characterising the surface of real machinery component which can be worn, for example.

2.2 Surface roughness generation

The greatest advantages of this method, in comparison with the measurement, are the high time-efficiency, no need for additional equipment (standard PC is sufficient) or unlimited possibilities for creation of the different surface patterns. The main disadvantage is the need to develop specialized software.

To generate rough surfaces based on fractal theory are used predominantly following methods: the midpoint displacement technique and the Weierstrass-Mandelbrot function.

The first mentioned method, described in detail in the source [4], finds mostly its application in the scans reconstruction of different fracture surfaces of various materials. For our purposes, modelling of the surface roughness of real machinery parts, the most suitable method seems to be the Weierstrass-Mandelbrot function. This function was published in 1998 by Yan and Komvopoulos [5] to generate the three dimensional rough surfaces. Fractal formations, which include the simulation of the resulting surface generated by this function, have their basis in a wide chaos theory pioneered by Benoit Mandelbrot himself [6].

The above mentioned Weierstrass-Mandelbrot function is expressed as:

$$z(x,y)=L\left(\frac{G}{L}\right)^{(D_f-2)}\left(\frac{\ln\gamma_f}{M}\right)^{1/2}\sum_{m=1}^{M}\sum_{n=0}^{n_{\max}}\gamma_f^{(D_f-3)n}\left\{\cos\phi_{m,n}-\cos\left[\frac{2\pi\gamma^n(x^2+y^2)^{1/2}}{L}\right]\cos\left(\tan^{-1}\left(\frac{y}{x}\right)-\frac{\pi m}{M}\right)+\phi_{m,n}\right\} \quad (1)$$

Where L is the sample length [m], G is the fractal roughness [m], D_f is the fractal dimension [-],γ_f is the scaling parameter [-], M is the number of superposed ridges used for the surface profile construction [-], n is the frequency index [-] and $\phi_{m,n}$ is the random phase [-].The upper limit of the frequency index can be determined by the formula:

$$n_{\max}=\text{int}\left[\frac{\log(L/L_S)}{\log\gamma_f}\right], \quad (2)$$

where int[…] denotes the maximum integer value of the number in the brackets and L_S is the cut off length.

Specific values of the variables will be discussed in the chapter 9.

When there is needed to generate the rough surface based on the measured data by using the fractal theory, it is essential to know one of the main inputs into the Weierstrass-Mandelbrot function, the fractal dimension D_f. That is why the next chapter describes functionality of the determination of fractal dimension.

3. FRACTAL DIMENSION ANALYSIS TOOL

3.1 Theoretical background

Although the fractal geometry is known since the 1970's there is no exact or universal definition of this concept. Mandelbrot defined fractal using its main feature, the self-similarity. This shows that fractal is created by infinite number of geometric patterns that repeat themselves in the basic body with the change of view scale. Fractal formation can be described with the use of two well-known examples: the Koch snowflake, or the length of the Britain coastline [8].

The fractal dimension can take non-integer values in range of $0<Df<3$. For example simple line would have fractal dimension of $Df=1$, the plain surface $Df=2$, but surface with fractal dimension of $Df=2.9$ would fill the space more like a volume.

3.2 Surfaces fractal dimension

Fractal dimension can be used to describe the complexity of the analysed surface, as it is shown in the next Figs. 1-2. Even though these two surfaces have the same roughness (Ra=0.8 μm), it can be clearly seen that they look different. This divergence is caused by the fractal dimension.

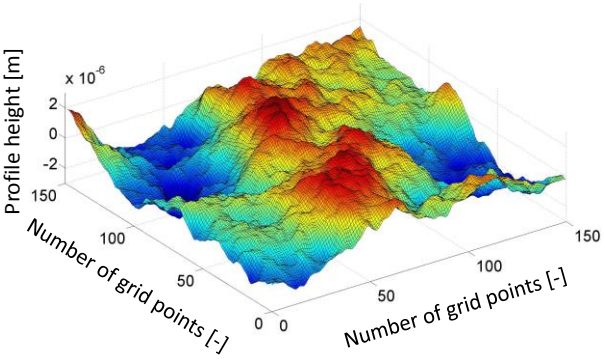

Fig. 1. Surface example with the fractal dimension 2.1

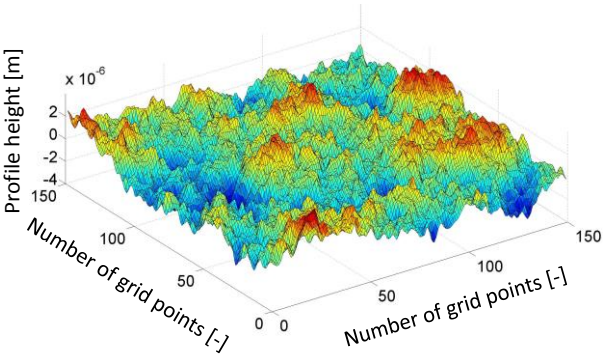

Fig. 2. Surface example with the fractal dimension 2.7

3.3 Computational algorithm

To determine fractal dimension (FD) the MATLAB script was developed, it can provide the real value of FD of given surface. As it was mentioned above, fractal geometry is a repetition of geometric patterns with the change of scale. This characteristic is used in the FD analysis tool which means that FD calculation is based on the surface area depending on the scale. For this purpose is the surface divided into known number of elements. For each element the area is calculated, which is summed up for the whole surface. The element size is gradually decreasing from the size equal to the size of surface multiplied by 0.9.

Because it is challenging to accurately determine FD, three different ways to calculate the area of one element were implemented. The reasons for this step will be explained further.

The first approach suggested by Kwaśny (2009) is described by following equation. [9]

$$A_i(\delta_e)=\frac{1}{2}\delta_e\left(\sqrt{{\delta_e}^2+(h_{ai}-h_{bi})^2+(h_{ci}-h_{bi})^2}+\sqrt{{\delta_e}^2+(h_{ai}-h_{di})^2+(h_{ci}-h_{di})^2}\right) \quad (3)$$

Where $A_i(\delta_e)$ is the area of the element number i [m^2], δ_e is the length of the element side [m], and h_{ai}, h_{bi}, h_{ci}, h_{di} are heights in corners of the element [m].

As a second approach the formula developed by Xie (1998) was implemented. [10]

$$A_i(\delta_e)=\frac{1}{2}\left(\sqrt{{\delta_e}^2+(h_{ai}-h_{di})^2}\sqrt{{\delta_e}^2+(h_{di}-h_{ci})^2}+\sqrt{{\delta_e}^2+(h_{ai}-h_{bi})^2}\sqrt{{\delta_e}^2+(h_{bi}-h_{ci})^2}\right) \quad (4)$$

Lastly, the third approach, based on Heron's formula for the calculation of the area of triangle, is expressed by the following equation.

$$A_i(\delta_e)=\sqrt{s_{abc}|s_{abc}-l_a||s_{abc}-l_b||s_{abc}-l_{ac}|}+\sqrt{s_{acd}|s_{acd}-l_{ac}||s_{acd}-l_c||s_{acd}-l_d|} \quad (5)$$

Where l_a, l_b, l_c and l_d are lengths of the element sides [m], s_{abc} and s_{acd} are the circumferences of the triangles created by dividing the element by its diagonal [m] and l_{ac} is the length of the element diagonal [m].

If the whole area of surface is known for the present element size, then these two parameters are plotted to the fully logarithmic axes graph and linear regression is performed on the linear part of the data set, as it is shown in the following Fig. 3.

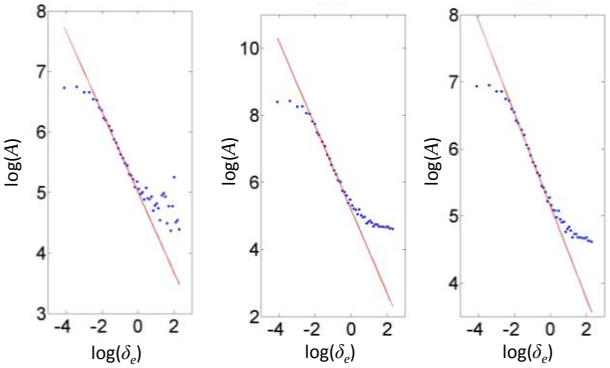

Fig. 3. Fully logarithmic interpretation of the surface area on the element size dependence. The left one: according the Kwaśny formula, the middle one: according the Xie approach and the right one: computation based on Heron's formula.

The line formed during linear regression can be described as:

$$y_f = \alpha_f + \beta_f x_f . \quad (6)$$

Then the FD of the analysed surface is calculated according to the equation: [9]

$$D_f = 2 - \beta_f . \quad (7)$$

These three formulae were used because: a) during the testing phase (with surfaces of known FD) of the FD analysis a tool was discovered, b) none of the formulae can be used for whole range of FDs (D_f=2.1 to 2.9), and c) neither of the formulae is accurate enough through the whole range.

However, soon was also discovered that the second formula (3) works well with low values of the FD (D_f < 2.2). It was also discovered that the most accurate results of higher FD values (D_f > 2.2) were obtained by calculating arithmetic mean value of the results of formulas (4) and (5).

After implementation of these changes to the FD analysis tool, the maximum error of value determining is within 1.5 %, instead of up to 12 % when only one formula is used. The effect of this improvement can be clearly seen on the graph below (Fig. 4).

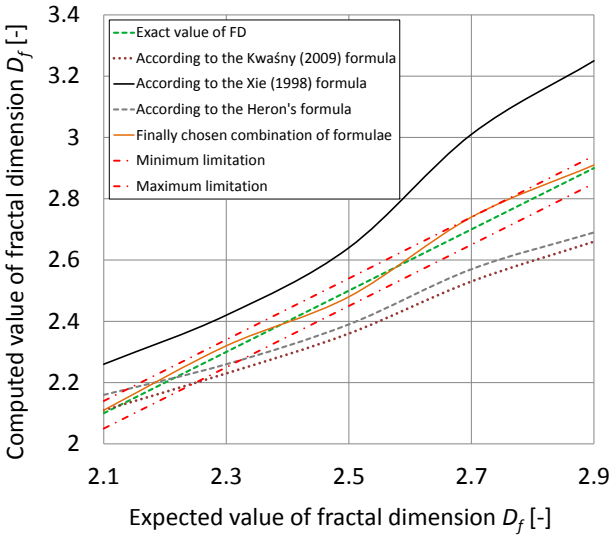

Fig. 4. The comparison of used approaches.

In many cases, where the implementation of formulas for calculating the contact pressure is realised, the Gaussian distribution of asperity heights is presumed. Therefore, even here, this analysis should not be left out.

4. NORMAL DISTRIBUTION TEST TOOL

Generally, statistical testing is based on the knowledge of sampling distribution of the measured or computed data. Usually, for further computation, it is assumed that data comes from the normal distribution and therefore this fact might be tested first. Normality testing is not that common because the average statistics that comes next is less sensitive on the normality distribution condition if the number of examples is higher than approximately 30. But still, it is a good example of the obtained data validation.

4.1 Chi-squared test of goodness of fit (Pearson's test)

Chi-squared test is one of the well-known tests that are used to check normality distribution of data. Fundamentally it is a comparison of the differences between the observed distribution function and the normal distribution function. X^2 test criterion assesses whether the difference in frequency counts are only accidental and examined data comes from the normal distribution or whether the variance is too high and the origin from the gauss distribution can be rejected. Criterion χ^2 is defined as follows:

$$\chi^2 = \sum_{i=1}^{m} \left(\frac{t_i - \tilde{t}_i}{\tilde{t}_i} \right)^2 . \quad (8)$$

Where t_i is observed frequency count in particular class m and $\tilde{t}_i$ is theoretical frequency count in particular class m.

If the amount of examined data is signed n_s, the sample average value of data x_s is μ_s and sample standard deviation is σ_s, then the theoretical frequency counts are defined as:

$$\tilde{t}_i = \left(\sum n_s \right) \cdot \left(\frac{x_{s_i}^{+} - \mu_s}{\sigma_s} - \frac{x_{s_{i-1}}^{+} - \mu_s}{\sigma_s} \right). \quad (9)$$

Quantification x^+ is gained from the division of examined data into frequency intervals. For example in interval <1,2> the considered value of x^+ is 2.

After the χ^2 number is computed, it must be compared with the critical value from the chi-squared distribution. When $\chi^2 < \chi^2_{crit}$, it means that the assumption of normal data distribution is approved. If $\chi^2 > \chi^2_{crit}$, the normal distribution origin can be neglected.

When such test of data normality is successfully done, other hypothesis testing can be certainly performed.

4.2 T-test (student's test)

Concerning surface roughness data which are computed using previously described formulas, some kind of validation is useful to know whether the given conditions were fulfilled or not. In this case it is tested that given roughness *R*a is statistically the same as the one computed from generated surfaces data (single t-test). Alternative test is about the surfaces couple, where is tested that the roughness *R*a of the couple is statistically the same (t-test for couples).

Hypothesis testing is common topic which is taught at every lecture of mathematical statistics. Therefore, no exact description of information sources is included. Normality testing is described in more detail because it is not used that frequently.

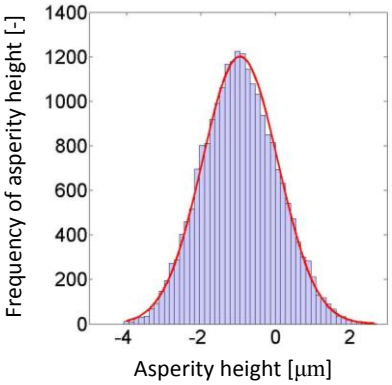

Fig. 5. Specific example of histogram of analysed surface.

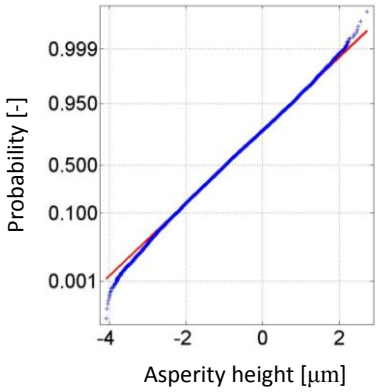

Fig. 6. Specific example of normal probability plot of analysed surface

5. DETERMINATION OF STATISTICAL PARAMETERS OF THE GENERATED SURFACE

Because of the random phase $\phi_{m,n}$, created by using random number generator function (a part of MATLAB) and has a range 0 to 2π, is each surface unique. Therefore, it is important to verify if the created surface possesses the expected values of asperity heights, areal density of asperities and average radius of the asperity curvature or the other statistical parameters, possibly useful as inputs for future contact modelling. For this purpose was created a set of special subroutines was created and also implemented into MATLAB programing environment.

5.1 Basic statistical characterization of surface roughness

Basic characterization of rough surfaces is described in the standards of each country. This theory is well described by formulae together with their digital expressions, for example in the source [7].

Furthermore, in the literature, generally, it is possible to find different naming of the basic statistical parameters for 2D and 3D surfaces. In this case, the 3D characterization of the rough surface (either measured or generated) is performed as of the 2D, always determined separately for each row and column. The resulting statistical characteristic is then simply their average.

However, everything depends on one basic definition of the so-called zero level line of the surface. The following paragraph will explain the principles of the code for the determination of the zero level line (plane) of a rough surface.

The core of algorithm for determination of zero level line for each line and column of the surface matrix can be based on numerical integral computation. Zero level line is located in the specific height of 2D surface profile whereas the positive area under surface profile (above zero level line) has the same area [m²] as the negative area (under the zero level line). Precision of described computational algorithm depends on configured error of this computation. Then until the correct compliance of above mentioned "while" cycle is done, the zero level line is shifted in correct direction. The comparison of the same 2D surface roughness profile (one after the generation and the second one after determination of the zero level line) is shown in the next figure. The difference is visible at the first glance.

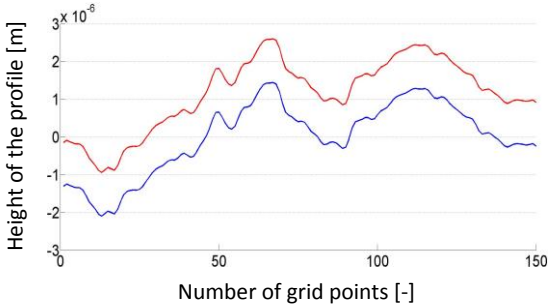

Fig. 7. Zero level determination of the 2D surface roughness profile

After the above described determination of the zero level line of the each column and the each line of 3D surface roughness profile follows the implementation of basic formulae and calculation of statistical parameters, see source [7]. The most widely used parameters for characterization of surface profile can be computed by following formulae.

$$Ra = \frac{1}{n}\sum_{i=1}^{n}|z_i| \tag{10}$$

$$Rq = \left(\frac{1}{n}\sum_{i=1}^{n}z_i^{\,2}\right)^{1/2} \tag{11}$$

Where *Ra* is the average absolute deviation from mean line of the surface roughness profile [m], n is the number of peaks over the sampling length, z is the actual height of each asperity [m] and *Rq* is the root mean square deviation from the mean line of the 2D profile [m].

5.2 Advanced statistical characterization of surface roughness

Inputs for computational modelling of frictional losses, e.g. of slide bearings, can consist of the information about areal density of asperities, or average radius of the curvature of the asperity peak. Therefore, determination of these two statistical parameters is described in following paragraphs.

For the purposes of determining the average curvature of asperities and their areal density, it is necessary to perform some kind of filtration at first. If the given local peak is about to be declared as the real peak, it must comply with following four conditions:

It must lie above the zero level line of the surface profile; it must be greater than the two adjacent grid points in both directions; the second derivative of the function (row or column) at a given point must be less than 0 (the function must be concave at that point); it must be a turning point of the function (it means that the behaviour of the analysed function here changes itself from increasing to decreasing function, or vice versa).

For the above mentioned conditions it is necessary to determine the first and the second numerical derivative of the function (each row and each column).

The final number of peaks is then considerably reduced. An illustrative example of such a reduction is shown in the following figure. Basis applicable examples of formulae for determining the numerical derivatives are also listed below.

The calculation is, of course, modified according to the position of the point in the matrix that is

calculated (for the calculation of the first point in the row the two previous points cannot be found).

$$\dot{f}(x_i)=\frac{f(x_{i+1})-f(x_i)}{h} \tag{12}$$

$$\ddot{f}(x_i)=\frac{f(x_{i+2})-2f(x_{i+1})-f(x_i)}{h^2} \tag{13}$$

Variables from eq. (12) and (13) are explained together with variables of the next equation.

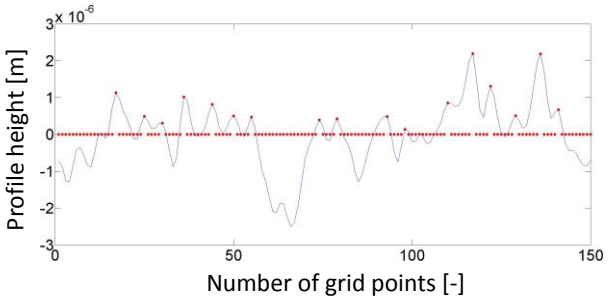

Fig. 8. View of the original 2D roughness profile with marked points of the resulting profile after filtering.

Then the areal density is simply determined by the number of points that meet these conditions, and by the size of the analysed sample of the surface.

The radius of curvature of the peak is then determined again over each row and column of the surface roughness matrix, which satisfy all the above mentioned conditions. It is a calculation of the osculating circle, which is governed by the following formula.

$$\beta_c=\frac{\left|\ddot{f}(x_i)\right|}{\sqrt{\left(1-\left(\dot{f}(x_i)\right)^2\right)^3}} \tag{14}$$

Where $\dot{f}(x_i)$ is the first numerical derivative of the analysed function at the point x_i of the function vector, $\ddot{f}(x_i)$ is the second numerical derivative of the analysed function at the point x_i of the function vector, and β_c is the curvature radius of the surface roughness peak at the point x_i of the function vector [m].

6. SURFACE ROUGHNESS DIRECTIONAL DEPENDENCE

Considering the [1], there is the directionality of analysed surfaces determined by the following equation describing areal autocorrelation function (AACF). The areal autocorrelation function gives the information about correlation between the original surface and the same surface shifted by m (n) – times differential length Δx (Δy) in all possible plane directions (+/- x and +/- y).

$$R(\tau_i,\tau_j)=\frac{1}{(M-i)(N-j)}\cdot \sum_{l=1}^{N-j}\sum_{k=1}^{M-i}\eta(x_k,y_l)\eta(x_{k+i},y_{l+j}) \tag{15}$$

In upper mentioned equation has i in range 0, 1 ..., M; and j in range 0, 1, ..., N; Whereas M and N is the mesh grid size of the analysed sample of measured or generated surface in x and y direction respectively. $\tau_i=i\cdot\Delta x$ and $\tau_j=j\cdot\Delta y$, where Δx and Δy is the differential length in x and y direction respectively. If the maximum number of grid points in the directions x and y is M, N respectively, then it is natural that the surface can be shifted maximally $M/2$ or $N/2$ – times respectively. Then m is in interval (0, $M/2$) and n is in interval (0, $N/2$).

The residual surface $\eta(x,y)$ and other required variables are computed by following equations.

$$\eta(x,y)=z(x,y)-(a+bx+cy) \tag{16}$$

Here:

$$a=\frac{(7MN+M+N-5)w}{MN(M+1)(N+1)}-\frac{6(N+1)u-6(M+1)v}{MN(M+1)(N+1)}, \tag{17}$$

$$b=\frac{12}{\Delta x}\cdot\frac{u-\frac{M-1}{2}w}{MN(M-1)(M+1)}, \tag{18}$$

$$c=\frac{12}{\Delta y}\cdot\frac{v-\frac{N-1}{2}w}{MN(N+1)(N+1)}. \tag{19}$$

Where:

$$u=\sum_{l=1}^{N}\sum_{k=1}^{M}(k-1)z(x_k,y_l), \tag{20}$$

$$v=\sum_{l=1}^{N}\sum_{k=1}^{M}(l-1)z(x_k,y_l), \tag{21}$$

$$w=\sum_{l=1}^{N}\sum_{k=1}^{M}z(x_k,y_l). \tag{22}$$

For the purpose of discovery of the analysed surface directionality is, primarily, necessary to know the number of grid points (length), needed for the reduction of AACF to the 50 % of its original height, in both directions. $\lambda_{x0.5}$ and $\lambda_{y0.5}$ [2]. For better illustration is just good to mention that for example in the source [3] is the reduction presented to the 10 % of original AACF height for the determination of surface roughness directionality. Then the directional dependence of surface roughness is computed by the following equation, presented in the source [2].

$$\gamma_R = \frac{\lambda_{x0,5}}{\lambda_{y0,5}} \tag{23}$$

For better illustration, what it approximately means, the value γ_R is given the following Fig. 9.

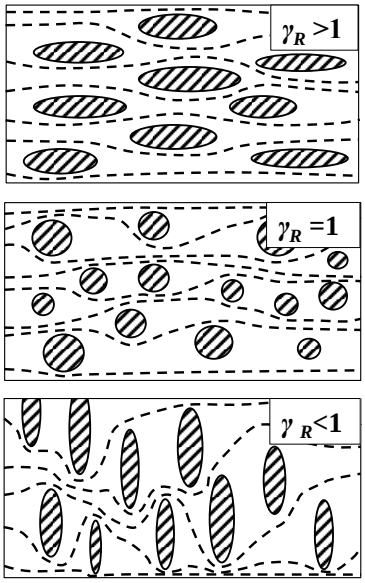

Fig. 9. Example of contact areas of longitudinally oriented (γ_R>1), isotropic (γ_R=1) and transversely oriented (γ_R<1) surfaces [2]

According to the equation (23) it is logical that 3D graphical representation of AACF of isotropic surface roughness is symmetrically shaped. The following picture presents a typical view of such AACF with 3D plot of the appropriate surface, Fig. 10.

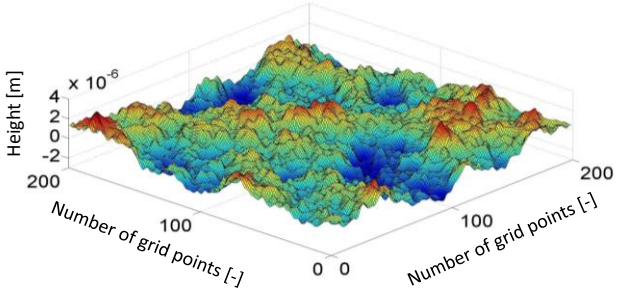

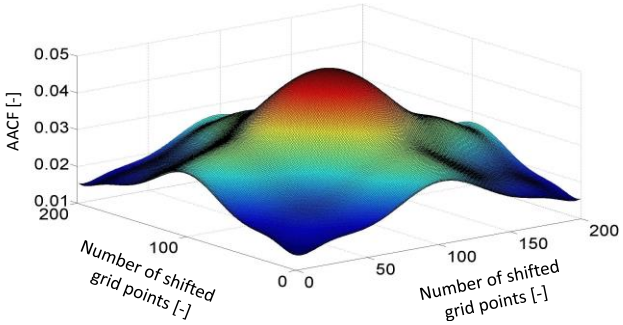

Fig. 10. Example of generated 3D surface roughness profile (upper) and it's according AACF.

All previously mentioned software tools have been created specifically for their further use in order to determine the effect of two approaching surfaces on the formation of the hydrodynamic lubricating layer. Then should be covered the behaviour of transition between the purely hydrodynamic lubrication regime and dry friction, as described by the Stribeck curve (Fig. 11).

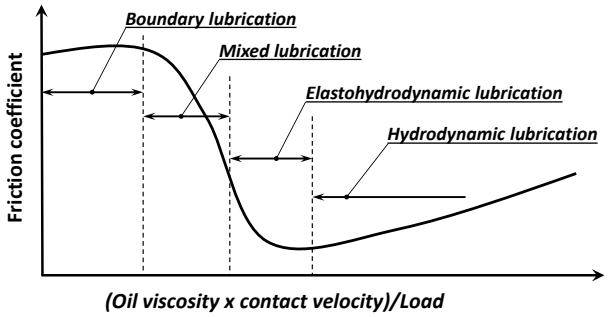

Fig. 11. Stribeck curve.

7. INFLUENCE OF SURFACE ROUGHNESS ON HYDRODYNAMIC LUBRICATION LAYER

Computational approach, which affects the above-mentioned connection between the mixed lubrication regime and the hydrodynamic regime, i.e., in our case, a description of the effect of surface roughness on the hydrodynamic pressure in the oil film layer, was published in 1978 by authors Nadir Patir and H.S. Cheng [2]. The above mentioned effect is incorporated by using factors of flow (flow factors) in the Reynolds equation. The resulting shape of this modified equation is then:

$$\frac{\partial}{\partial x}\left(\phi_x \frac{\rho h^3}{12\eta}\frac{\partial p}{\partial x}\right)+\frac{\partial}{\partial y}\left(\phi_y \frac{\rho h^3}{12\eta}\frac{\partial p}{\partial y}\right)= \frac{U_1+U_2}{2}\frac{\partial(\rho h_T)}{\partial x}+\frac{U_1-U_2}{2}\sigma\frac{\partial(\rho\phi_s)}{\partial x}+\frac{\partial(\rho h_T)}{\partial t} \tag{24}$$

Here h denotes the thickness of the oil film layer [m], h_T is the local oil film thickness [m], x, y denote the coordinate, t is the time [s], p is the pressure [Pa], ρ is the density of the oil [kg·m^{-3}] η is the dynamic viscosity of the oil [Pa·s], σ is a combined arithmetic mean roughness of both surfaces [m], U_1, U_2 is the circumferential speed of surface 1 resp. 2 [m·s^{-1}] and ϕ_x, ϕ_y and ϕ_s are just those flow factors [-]. The situation is well illustrated by the following Fig. 12.

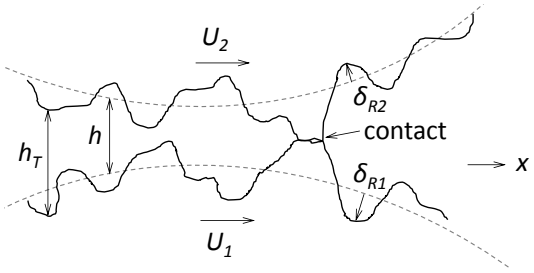

Fig. 12 The oil film thickness in micro scale [2].

Previous equation can be used for both isotropic surfaces and surfaces with different directionally oriented surface asperities. Flow factors are for these surfaces expressed via empirical relationships as a function of the ratio h/σ and the surface characteristics γ_R. Determination of the variable γ_R is described in detail in the previous chapter.

If there is no scan of the surface, if details of manufacturing process of the surface structure are unknown, or if we are simply not interested in high precision of our computation, then empirical equations can be advantageously used for calculation of the flow factors mentioned in the sources [2]. However, the following passage will deal with the converse case where we want to describe in detail the behaviour of the thin lubrication layer between two specified contact surfaces. For this purpose, it is necessary to use other specialized computational tool.

7.3 Flow factors calculation tool

Basically, the computation works on the principle of pre-calculated databases of flow factors. For given surfaces (either generated or measured) the calculation of flow factors for different values of their basic distances is done – the distance h (determined from the surface zero level plane) which adequately covers the range of values that can occur in reality. Then, from the pre-calculated databases it is possible to inter or extrapolate the final value of flow factor. Examples of such pre-calculated databases are listed in the chapter 9. EXAMPLES OF RESULTS.

The calculation is based on the numerical solution of Reynolds equation. The flow between two rough surfaces which are separated from each other by the space h_T, is solved. Rough surfaces are there just because of the micro-scale determination of the h_T matrix. If that surface protrusions are in contact, the distance matrix of these surfaces there reaches 0 at these grid points. In practice it means that no lubricant flow occurs at this grid point.

The Flow factors then represent something like a loss coefficient of the lubricant flow in the defined gap between surfaces. Furthermore, this information (about numbers of non-lubricant flow points) can be used for the future calculation of a contact pressure (for a given number of h/σ ratio the number of contact points at given area and for given type of surface is known).

To solve the Reynolds equation from above, it is also necessary to define the boundary conditions of the solution. Example of the Reynolds equation, dimensionless variables, the resulting expression of discretized formula for pressure calculation, and formulas for calculation of flow factors follow.

$$\frac{\delta}{\delta x}\left(h_T{}^3\frac{\delta p}{\delta x}\right)+\frac{\delta}{\delta y}\left(h_T{}^3\frac{\delta p}{\delta y}\right)=6\eta U\frac{\delta h_T}{\delta x} \quad (25)$$

$$H=\frac{h_T}{\sigma}, X=\frac{x}{\sigma}, Y=\frac{y}{\sigma}, P=p\sigma, \bar{\eta}=\frac{\eta}{\eta_0} \quad (26)$$

Here the h_T denotes the local oil film thickness [m], x, y are the coordinates, p is the pressure [Pa], η is the oil dynamic viscosity [Pa·s], σ is the combined arithmetic mean roughness of both surfaces [m], U is the combined circumferential speed of surfaces [m·s^{-1}] and H, X, Y, P and $\bar{\eta}$ are the dimensionless variables.

After discretization the final equation for description of the pressure can be in following shape:

$$P_{(i,j)} = \frac{6\bar{\eta}U\dfrac{H_{\left(i+\frac{1}{2},j\right)} - H_{\left(i-\frac{1}{2},j\right)}}{\triangle X}}{D} - \frac{\dfrac{H^3_{(i-\frac{1}{2},j)}P_{(i-1,j)} + H^3_{(i+\frac{1}{2},j)}P_{(i+1,j)}}{(\triangle X)^2}}{D} - \frac{\dfrac{H^3_{(i,j+\frac{1}{2})}P_{(i,j+1)} + H^3_{(i,j-\frac{1}{2})}P_{(i,j-1)}}{(\triangle Y)^2}}{D} \quad (27)$$

Where:

$$D = \frac{\left(-H^3_{(i+\frac{1}{2},j)} - H^3_{(i-\frac{1}{2},j)}\right)}{(\triangle X)^2} + \frac{\left(-H^3_{(i,j+\frac{1}{2})} - H^3_{(i,j-\frac{1}{2})}\right)}{(\triangle Y)^2}. \quad (28)$$

Equations for the pressure flow factor calculation in direction x (Φ_x), y (Φ_y) and for the shear flow fac. Φ_s are:

$$q_{rough\_x} = -\frac{{h_T}^3}{12\eta}\frac{dp}{dx} + \frac{Uh_T}{2}, \quad (29)$$

$$q_{rough\_y} = -\frac{{h_T}^3}{12\eta}\frac{dp}{dy} + \frac{Uh_T}{2}, \quad (30)$$

$$q_{smooth\_x} = -\frac{h^3}{12\eta}\frac{dp}{dx}, \quad (31)$$

$$q_{smooth\_y} = -\frac{h^3}{12\eta}\frac{dp}{dy}, \quad (32)$$

$$\phi_x = \frac{q_{rough\_x}}{q_{smooth\_x}}, \quad (33)$$

$$\phi_y = \frac{q_{rough\_y}}{q_{smooth\_y}}, \quad (34)$$

$$\phi_s = \frac{\dfrac{2}{L_x L_y}\int_0^{L_y}\int_0^{L_x}\left(-\dfrac{{h_T}^3}{12\eta}\dfrac{dp}{dx}\right)dxdy}{U\sigma}. \quad (35)$$

Here the variables q are the flow of the oil between two surfaces.

These equations demonstrate that flow factors are expressed as a ratio between the flow through rough surfaces and the flow through smooth surfaces. For calculation of these pressure flow factors was used the first boundary condition – that the surfaces are in not in a relative movement (U=0). The second boundary condition regards the pressure at the beginning and at the end of the analysed element (P_{in} and P_{out}). P_{in}=1e5 Pa, P_{out}=0 Pa. For calculation of the flow between rough surfaces (q_{rough}) the equation (27) is used (determination of the pressure loss). In the case of smooth surfaces the pressure loss is linearly distributed between P_{in} and P_{out}.

For calculation of above expressed shear flow factor the first boundary condition was used – that the surfaces are in a relative movement (U=1.5 m/s). The second boundary condition is P_{in}= P_{out}=0 Pa. L_x, L_y is the length of the analysed surface sample [m].

Above described tool for flow factors calculation was again implemented in programing environment MATLAB. The numerical solution is based on finite difference method as well as the other software tools described in this article which utilize the iterative solution.

The equations from (29) to (35) are taken from sources [14], [15], [16].

Example of computed hydrodynamic pressure matrix for pressure flow factor calculation is demonstrated in the following Fig. 13.

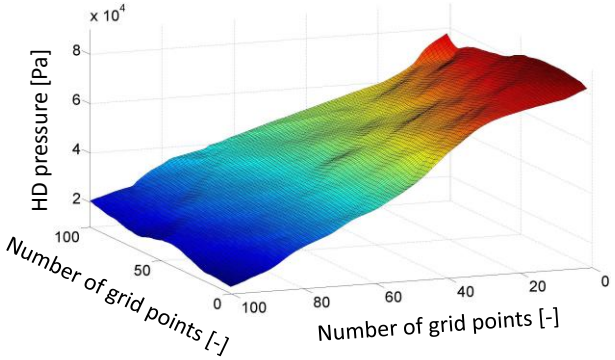

Fig. 13. Example of hydrodynamic pressure matrix for ϕ_x calculation

8. FRICTIONAL LOSSES DETERMINATION

There are two basic approaches applicable to determination of frictional losses. The first mentioned approach presented in this paper is well known and still in use. Inputs into this model are created by variables described in detail in previous chapters and also by outputs from the hydrodynamic solution. Used hydrodynamic solution is fully described in [12], written by Novotný, co-author of this paper.

8.1 Greenwood and Tripp approach

Computational model described in this chapter is based on the theory explained in detail in [11]. The basic equation for the calculation of the contact pressure has following form:

$$p(d)=\frac{8\pi}{5}(\eta\beta_c\sigma)KF_{5/2}\left(\frac{d}{\sigma}\right). \quad (36)$$

Where:

$$K=\frac{2\sqrt{2}}{3}(\eta\beta_c\sigma)E'\sqrt{\left(\frac{\sigma}{\beta_c}\right)}, \quad (37)$$

$$\sigma=\sqrt{Sq_1^2+Sq_2^2}\quad , \quad (38)$$

$$\frac{1}{E'}=\frac{1-\upsilon_1^2}{E_1}+\frac{1-\upsilon_2^2}{E_2}. \quad (39)$$

Here η is the surface density of the roughness peaks [1/m^2], β_c is the radius of curvature [m], σ is the average roughness of surfaces [m], ν is the Poisson constant of materials [-], Sq is the root mean square deviation from the mean plane of the 3D profile [m], E' is the composite elastic modulus [Pa], E is the elastic modulus of materials [Pa] and $F_{5/2}$ is the roughness contact pressure function [-].

Then, the total value of the pressure is given by the sum of the hydrodynamic pressure and the pressure, which is given by the contact between asperities of two surfaces. This can be expressed by the following equation.

$$P_{Total}=P_{Hydrodynamic}+P_{Contact} \quad (40)$$

From the element size it is possible to compute the whole area of the contact. Then, from the determined contact pressure, it is relatively easy to express the contact force or the friction torque (as regards the rotary part).

The contact pressure curve, depending on the ratio of lubrication height and the variable sigma (h/σ), is in this case very nonlinear. It can cause, especially in case of very thin lubrication layer, extensive challenges. Therefore, it is also good to consider a different computational model and then compare results. Good and stable results are possible to obtain from one also very old and well-known theory – the Hertz theory. In this case the contact between the plate and the sphere is taken into consideration. A smaller nonlinearity in the contact pressure curve of this model can help a lot in online calculation, in the multi body system (MBS) application.

8.2 Application of the Hertz theory

This theory can be described by the following set of equations.

$$\delta=|\sigma-h|,\ R=\beta_c{}^2/2\beta_c, \quad (41)$$

$$W=\frac{\sqrt{\delta^3E'^2R\dfrac{1}{1.0397^3}}}{N_a},\ a=\left(\frac{3WR}{E'}\right)^{1/3}, \quad (42)$$

$$P_{\max}=\frac{3W}{2\pi a^2},\ P=\frac{W}{\pi a^2}. \quad (43)$$

Where δ is the deflection at the centre of the contact [m], R is the reduced radius of curvature [m], β_c is the radius of curvature [m], W is the normal load [N], E' is the composite elastic modulus [Pa], N_a is the number of asperities per element size, computed from the variable η (the surface density of the roughness peaks [1/m^2]), a is the radius of contact area [m] and P, P_{max} are contact pressures [Pa]. Above mentioned formulae can be found in source [13].

With application of the Hertz theory it is necessary to accept the following simplifying assumptions. Bodies in the contact are assumed to be isotropic and elastic, perfectly smooth and the contact areas are taken to be relatively flat and small to the radius of the non-deformed bodies' curvature.

9. EXAMPLES OF RESULTS

Results which are shown in the following three Figs. 14-16 were computed for surfaces generated by using fractal approach described in one of the introductory chapters. Statistical conformity of

generated surfaces was verified and all flow factors were computed twenty times. The same procedure was implemented for surfaces gained from measurement. Results are then averages from all computed values. Inputs into Weierstrass-Mandelbrot function for obtaining surfaces with *Sa* = 0.8 are listed in the Table 1.

Table 1. Used inputs for the surface roughness generation.

D_f	2.1	2.3	2.5	2.7	2.8	2.9
G	7.60E-17	1.85E-08	1.98E-07	5.15E-07	6.22E-07	7.10E-07
γ	1.5					
M	10					
L	3.00E-04	1.00E-04				
L_s	L /45					
n_{min}	0					
m_{max}	M					
m_{min}	1					

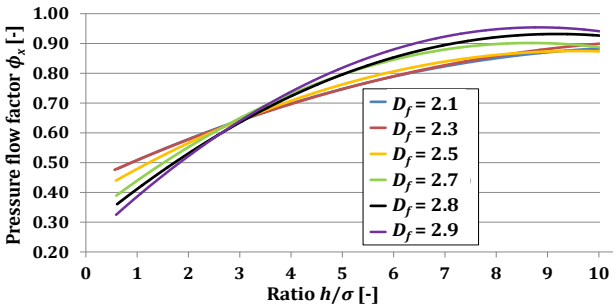

Fig. 14. Comparison of the pressure flow factors curves in x direction for different surfaces.

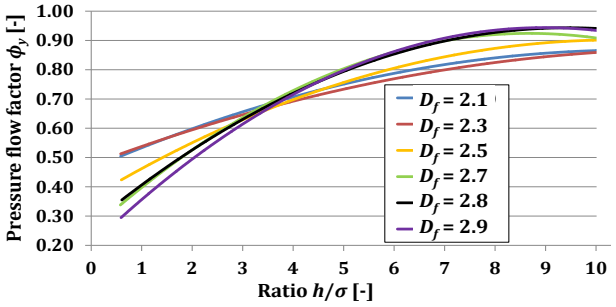

Fig. 15. Comparison of the pressure flow factors curves in y direction for different surfaces.

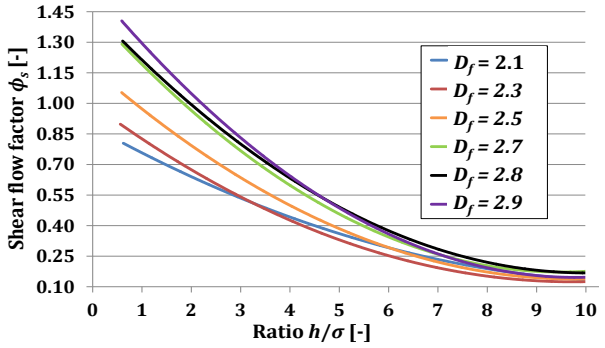

Fig. 16. Comparison of the shear flow factors curves in x direction for different surfaces.

Example of result in the Fig. 17 illustrates how different shape the curve representing the friction torque of a slide bearing can have, if the hydrodynamic or mixed lubrication regime is taken into account during the computational modelling of the slide bearing. As it is evident from the maximal values of the both curves, the one representing the asperity contact part reaches considerable values in the area of the maximum relative eccentricity of the bearing pin. In the modern powertrain development taking into account also the mixed lubrication regime is therefore practically necessary.

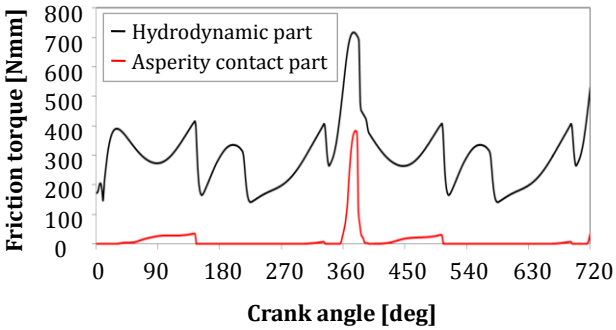

Fig. 17. Computational approaches comparison.

Behaviour of the directionally dependent surfaces can be analysed easily just by loading the appropriate scan of current surfaces. Examples of real scanned technical surfaces are depicted in the following Figs. 18-23.

Fig. 18. The compression piston ring.

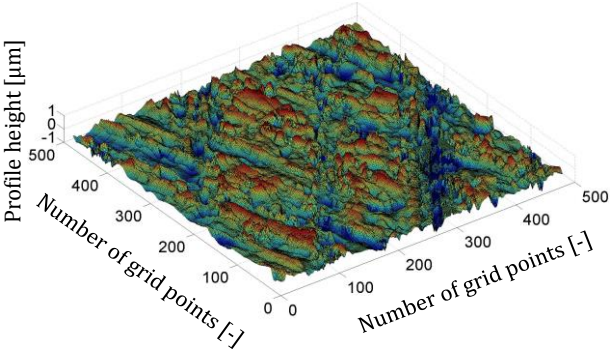

Fig. 19. The piston ring surface pattern.

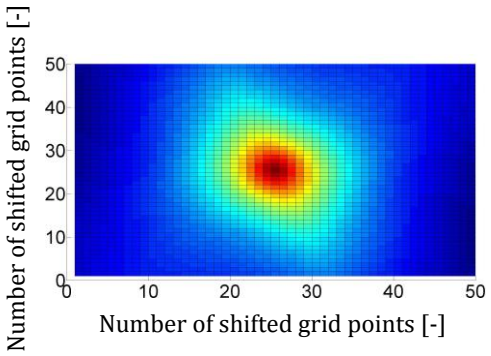

Fig. 20. The AACF representation of the piston ring surface pattern.

Fig. 21. The combustion engine slide bearing.

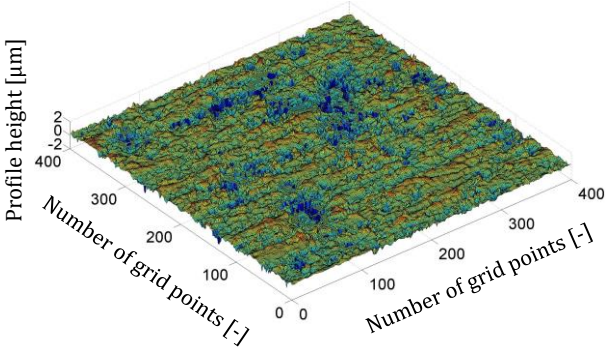

Fig. 22. The slide bearing shell surface pattern.

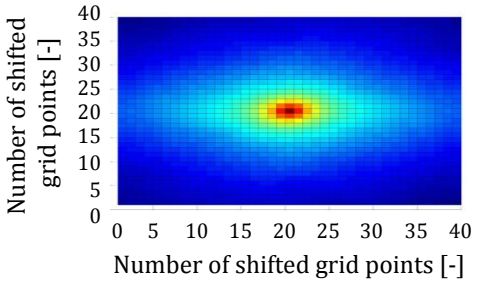

Fig. 23. The AACF representation of slide bearing shell surface pattern.

10. CONCLUSION

Contact mechanics is a frequently studied field. Many scientists around the world have been devoting large amounts of resources, effort and time into the development of different methods of the surface characteristics measurement, or to precisely analyze their behavior under heavy load in modern machineries. Therefore, in this paper the complex computational strategy for the detailed design of different machinery parts was described.

The authors in this article assembled the main challenges of each individual part of the software tools developed with a belief that a wide range of experts will become familiar with the existence of this methodology for different machine parts design. Hopefully, this would help to develop environmentally friendly, improved, and more efficient machines capable to save energy, time, and money.

Because all of the above introduced and described software tools are modular, they can be used for example for design or optimization of piston rings, journal or rolling bearings, etc. The presented theory is easily transferable to all machine components design.

Detailed information on the contact behavior of surfaces are advantageous and can be used for wear prediction which should also be very important for all experienced designers of all modern machines.

Acknowledgment

Outputs of this project, named NETME CENTRE PLUS (LO1202), were created with financial support from the ministry of education, youth and sports of the Czech Republic under the program supporting research, experimental development and innovation: "National Sustainability Programme I." The authors gratefully acknowledge this support.

REFERENCES

[1] K. Stout, et al.:*The development of methods for the characterisation of roughness in three dimensions*, Luxembourg: Office for Official Publications of the European Communities on behalf of the Commission of the European Communities, 1993.

[2] N. Patir, H. Cheng: *An Average Flow Model for Determining Effects of three-Dimensional Roughness on Partial Hydrodynamic Lubrication*, ASME Journal of Lubrication Technology, Vol. 100, No. 1, pp. 12-17, 1978.

[3] L. Lunde, K. Tonder: *Pressure and Shear Flow in a Rough Hydrodynamic Bearing, Flow Factor Calculation*, Journal of Tribology, Vol. 119, No. 3, pp. 549-555, 1997.

[4] J. Russ: *Fractal Surfaces,* New York: Plenum Press, 1994.

[5] W. Yan, K. Komvopoulos: *Contact analysis of elastic-plastic fractal surfaces*, Journal of applied physics, Vol. 84, No. 7, pp. 3617-3624, 1998.

[6] J. Gleick: *Chaos: making a new science*. London: Minerva, 1987.

[7] T. Thomas: *Characterization of surface roughness*, Precision Engineering, Vol. 3, No. 2, pp. 97-104, 1981.

[8] B. Mandelbrot: *Fractal geometry of nature*. New York: Freeman and company, 1983.

[9] W. Kwaśny: *A modification of the method for determination of surface fractal dimension and multifractal analysis*, Journal of Achievements in Materials and Manufacturing Engineering, Vol. 33, No. 2, pp. 115-125, 2009.

[10] H. Xie, J. Wang, E. Stein: *Direct fractal measurement and multifractal properties of fracture surfaces*, Physics Letters A, Vol. 242, No. 1-2, pp. 41-50, 1998.

[11] J. Greenwood, J. Tripp: *The contact of two nominally flat rough surfaces*, in: *Proceedings of the Institution of Mechanical Engineers 1847-1982*, Vol. 185, No. 1970, pp. 625-634, 1970.

[12] P. Novotný: *Virtual Engine – A Tool for Powertrain Development*, Brno: Brno University of Technology Inaugural Dissertation, 2009.

[13] G. Stachowiak: *Engineering tribology*. 4th ed. Oxford: Butterworth-Heinemann, 2014.

[14] L. Lunde, K. Tonder: *Pressure and Shear Flow in a Rough Hydrodynamic Bearing, Flow Factor Calculation*, Journal of Tribology, Vol. 119, No. 3, pp. 549-555, 1997.

[15] N. Letalleur, F. Plouraboué, M. Prat: *Lubricant flow between rough surfaces in sliding motion*, Revue de Métallurgie, Vol. 98, No. 5, pp. 455-458, 2001.

[16] H. Peeken, G. Knoll, A. Rienäcker, J. Lang, R. Schönen: *On the Numerical Determination of Flow Factors*, Journal of Tribology, Vol. 119, No. 2, 1997.